Bulletin of Mathematical Biology Vol. 50, No. 5, pp. 465–491, 1988.
Printed in Great Britain.

0092-8240/88$3.00+0.00
Pergamon Press plc

EXPLOSIVE ROUTE TO CHAOS THROUGH A FRACTAL TORUS IN A GENERALIZED LOTKA–VOLTERRA MODEL

■ NIKOLA SAMARDZIJA and LARRY D. GRELLER*
E. I. du Pont de Nemours & Co.,
Engineering Department, and
Central Research & Development Department,
Experimental Station,
Wilmington, DE 19898, U.S.A.

The behavior of a model that generalizes the Lotka–Volterra problem into three dimensions is presented. The results show the analytic derivation of stability diagrams that describe the system's qualitative features. In particular, we show that for a certain value of the bifurcation parameter the system instantly jumps out of a steady state solution into a chaotic solution that portrays a fractal torus in the three-dimensional phase space. This scenario is referred to as the explosive route to chaos and is attributed to the non-transversal saddle connection type bifurcation. The stability diagrams also present a region in which the Hopf type bifurcation leads to periodic and chaotic solutions. In addition, the bifurcation diagrams reveal a qualitative similarity to the data obtained in the Texas and Bordeaux experiments on the Belousov–Zhabotinskii chemical reaction. The paper is concluded by showing that the model can be useful for representing dynamics associated with biological and chemical phenomena.

Introduction. The original Lotka–Volterra model (Lotka, 1920; Volterra, 1931), for biological competition between two species was generalized by Smale (1976) for dimensions $n \geqslant 3$. He demonstrated that a population evolution of five or more biological species in competition can produce arbitrary dynamical behavior. In particular, Smale shows that for $n \geqslant 5$ the dynamical system may exhibit strange, or chaotic, type attractors. The last was strengthened by Arnéodo *et al.* (1982), by demonstrating that Smale's conditions can be preserved for strange attractors created through the interaction of four competing species. In addition, May *et al.* (1975), have reported on a three-dimensional competitive system that exhibits nonperiodic population oscillations of bounded amplitude and ever increasing cycle time. Bifurcations in three-dimensional competitive models were investigated by Gardini *et al.* (1986). By weakening the conditions of the Smale system, Arnéodo *et al.* (1980), have demonstrated further that one can obtain strange attractors in $n = 3$. This was observed also by Gilpin (1979) and Schaffer (1985) in a predator–prey type model.

* Permanent address: Information Industries, Inc., 8880 Ward Parkway, Kansas City, MO 64114, U.S.A.

The objective of this paper is to extend the work reported by proposing a three-dimensional generalization of the Lotka–Volterra model that is different from the systems addressed previously. The system proposed is

$$\Sigma: \quad \begin{aligned} \dot{X} &= X - XY + CX^2 - AZX^2 \\ \dot{Y} &= -Y + XY \\ \dot{Z} &= -BZ + AZX^2 \end{aligned} \tag{1}$$

where the relations between X and Y form the Lotka–Volterra expressions, while the relations between X and Z generalize the latter in three dimensions, and where $A, B, C \geqslant 0$. In this model, the parameters A, B and C will be analyzed in order to determine bifurcation properties of Σ. By investigating this system we shall also address complex oscillatory phenomena that currently are studied in the literature, e.g. Lorenz (1963), Rössler (1976) and Sparrow (1982). In particular, the phenomenon of chaos evolving on a fractal torus, such as reported by the Richetti *et al.* (1987), will be analyzed by analytically derived two-dimensional stability diagrams. These diagrams will reveal other interesting qualitative features of the system. Further, it is our intention to demonstrate that Σ fits a biological and chemical reaction scheme, and thus can be used to model dynamics involving species X, Y and Z. At this point it is worth noting that Σ does not satisfy Smale's condition 2 (1976). This implies that the proposed system allows positive feedback among the species. In addition, Σ is a two-predator/one-prey model, while the systems described in (Arnéodo *et al.*, 1980; Gilpin, 1979; Schoffer, 1985) are one-predator/two-prey models.

In the first part of the presentation, the analytic treatment of equation (1) is presented. Some classical results from the Lotka–Volterra model (Davis, 1962; Lotka, 1920; Nicolis and Prigogine, 1977; Volterra, 1931) will be generalized to the three-dimensional structure. At this stage, analysis will include evaluation of first-order behavior about steady state solutions. Also, useful geometric properties of (1) are discussed. The analytic treatment is concluded by discussion of the global behavior of Σ.

Next, two-dimensional stability diagrams are evaluated. The results are used to justify the existence of chaos in Σ as well as to demonstrate the explosive route to chaos. This route to chaos was also observed by Devaney (1987) for discrete-time systems. The section is concluded by illustrating chaotic trajectories that evolve on a fractal torus for different chaotic regions and by presenting numerically computed diagrams built from Poincaré planes. In addition, the results will be compared to those reported by the Texas (Turner *et al.*, 1981) and Bordeaux (Argoul *et al.*, 1987; Richetti *et al.*, 1987) groups. They investigated theoretically and experimentally the qualitative behavior of the Belousov–Zhabotinskii chemical reaction.

Finally, the results obtained are used to study the kinetics of a biological and chemical reaction scheme. The parameters A, B and C will become rate constants that affect the dynamics of constituents X, Y and Z. By understanding stability diagrams, one will be able to determine conditions for which a cooperation among the three species results in steady, periodic, or chaotic behavior. Also, in this section Σ will be generalized to allow for higher-order biological or chemical interactions to occur. We conclude by comparing the system's qualitative features with some well known experimental results in biology and chemistry.

1. Analysis of Proposed System.

First-order analysis. Let $\mathbf{S}\in\mathbf{R}^3$ be such that $\mathbf{S}=[X, Y, Z]^{\mathrm{T}}$. Then one can derive the following steady state solutions for Σ:

$$\mathbf{S}_{s1}=\begin{matrix}0\\0\\0\end{matrix};\quad \mathbf{S}_{s2}=\begin{matrix}1\\1+C\\0\end{matrix};\quad \mathbf{S}_{s3}=\begin{matrix}\sqrt{B/A}\\0\\(1+C\sqrt{B/A})/\sqrt{AB}\end{matrix};$$

$$\mathbf{S}_{s4}=\begin{matrix}-1/C\\0\\0\end{matrix};\quad \mathbf{S}_{s5}=\begin{matrix}-\sqrt{B/A}\\0\\(C\sqrt{B/A}-1)/\sqrt{AB}\end{matrix}.$$

Because we intend to interpret Σ as a chemical, biochemical, or ecological model, steady states $\mathbf{S}_{s4}$ and $\mathbf{S}_{s5}$ are not considered since they contain negative values for the species X. Also, in the presentation we require that $A, B, C\geqslant 0$.

Let $J(\mathbf{S})$ be the Jacobian of Σ, evaluated at $\mathbf{S}\in\mathbf{R}^3$. Furthermore, define $\Gamma\{J(\mathbf{S})\}$ and $\mathbf{W}\{J(\mathbf{S})\}$ to be, respectively, eigenvalue and associated eigenvector sets of $J(\mathbf{S})$, with one-to-one component correspondence. Then, the first-order stability about the steady state solutions is determined by the following sets:

$$\Gamma\{J(\mathbf{S}_{s1})\}=\{1, -1, -B\};\quad \mathbf{W}\{J(\mathbf{S}_{s1})\}=\left\{\begin{bmatrix}1\\0\\0\end{bmatrix},\begin{bmatrix}0\\1\\0\end{bmatrix},\begin{bmatrix}0\\0\\1\end{bmatrix}\right\} \tag{2}$$

$$\Gamma\{J(\mathbf{S}_{s2})\}=\{A-B, (C+\sqrt{(C-2)^2-8})/2, (C-\sqrt{(C-2)^2-8})/2\}$$

$$\mathbf{W}\{J(\mathbf{S}_{s2})\} = \left\{ \begin{bmatrix} 1 \\ (C+1)/(A-B) \\ \dfrac{B+C-A+(C+1)/(B-A)}{A} \end{bmatrix}, \right.$$

$$\left. \begin{bmatrix} 1 \\ \dfrac{C-\sqrt{(C-2)^2-8}}{2} \\ 0 \end{bmatrix}, \begin{bmatrix} 1 \\ \dfrac{C+\sqrt{(C-2)^2-8}}{2} \\ 0 \end{bmatrix} \right\} \tag{3}$$

and

$$\Gamma\{J(\mathbf{S}_{s3})\} = \{(\sqrt{B/A}-1), \quad (-1+\sqrt{1-8B(1+C\sqrt{B/A})})/2,$$
$$(-1-\sqrt{1-8B(1+C\sqrt{B/A})})/2\}$$

$$\mathbf{W}\{J(\mathbf{S}_{s3})\} = \left\{ \begin{bmatrix} 1 \\ -1-\dfrac{2\sqrt{AB}(1+C\sqrt{B/A})}{\sqrt{B/A}-1} \\ \dfrac{2(1+C\sqrt{B/A})}{\sqrt{B/A}-1} \end{bmatrix}, \right.$$

$$\left. \begin{bmatrix} 1 \\ 0 \\ \dfrac{-1-\sqrt{1-8B(1+C\sqrt{B/A})}}{2B} \end{bmatrix}, \begin{bmatrix} 1 \\ 0 \\ \dfrac{-1+\sqrt{1-8B(1+C\sqrt{B/A})}}{2B} \end{bmatrix} \right\}. \tag{4}$$

The geometric illustration of the three steady state solutions and their respective eigenvector sets is shown in Fig. 1.

In order to characterize a local behavior about a steady state $\mathbf{S} \in \mathbf{R}^3$, the definitions based on the properties of $\Gamma\{J(\mathbf{S})\}$ are given in Table I. These results are used to describe the steady state points $\mathbf{S}_{s1}$, $\mathbf{S}_{s2}$ and $\mathbf{S}_{s3}$ in terms of parameters A, B and C. It is easy to conclude that $\mathbf{S}_{s1}$ is a saddle point (index 1) for all A, B and C. However, the points $\mathbf{S}_{s2}$ and $\mathbf{S}_{s3}$ are characterized in Tables II and III.

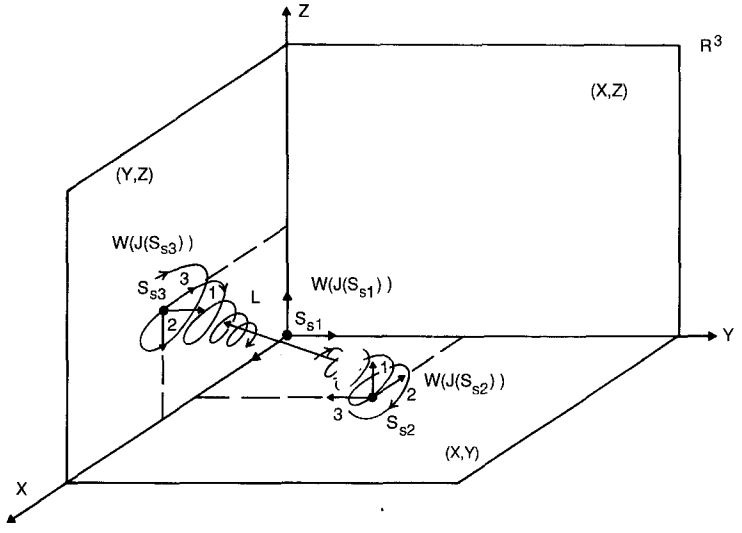

Figure 1. Geometric illustration of steady state solutions and their respective eigenvector positions. Indices 1, 2 and 3 indicate the first, second and third component in $\mathbf{W}\{J(\mathbf{S})\}$. The vortices indicate a behavior when $\mathbf{W}\{J(\mathbf{S})\}$ sets contain complex elements. The line L shows the action between $\mathbf{S}_{s2}$ and $\mathbf{S}_{s3}$.

TABLE I

	Types of steady states in $\mathbf{R}^3$	$\Gamma\{J(\mathbf{S})\}=\{\lambda_1,\lambda_2,\lambda_3\in\mathbf{R}$; s.t. $\lambda_1\geqslant\lambda_2\geqslant\lambda_3\}$	$\Gamma\{J(\mathbf{S})\}=\{\lambda_1\in\mathbf{R}$, $\lambda_2,\lambda_3\in\mathbf{C}$; s.t. $\lambda_3=\lambda_2^*\}$
	Unstable node	$\lambda_1,\lambda_2,\lambda_3\geqslant 0$	—
	Stable node	$\lambda_1,\lambda_2,\lambda_3\leqslant 0$	—
	Unstable saddle	$\lambda_1,\lambda_2>0$ and $\lambda_3<0$	—
	Stable saddle	$\lambda_1>0$ and $\lambda_2,\lambda_3<0$	—
x	Inward unstable vortex	—	$\lambda_1<0$ and $Re\{\lambda_2\}>0$
x	Inward nilpotent vortex	—	$\lambda_1<0$ and $Re\{\lambda_2\}=0$
x	Inward stable vortex	—	$\lambda_1<0$ and $Re\{\lambda_2\}<0$
x	Outward unstable vortex	—	$\lambda_1>0$ and $Re\{\lambda_2\}>0$
x	Outward nilpotent vortex	—	$\lambda_1>0$ and $Re\{\lambda_2\}=0$
x	Outward stable vortex	—	$\lambda_1>0$ and $Re\{\lambda_2\}<0$
xx	Unstable center	—	$\lambda_1=0$ and $Re\{\lambda_2\}>0$
xx	Nilpotent center	—	$\lambda_1=0$ and $Re\{\lambda_2\}=0$
xx	Stable center	—	$\lambda_1=0$ and $Re\{\lambda_2\}<0$

x. A vortex is a geometric complex in $\mathbf{R}^m$, $m\geqslant 3$. When it exists in a neighborhood of a steady state solution $\mathbf{S}\in\mathbf{R}^3$, then $J(\mathbf{S})$ has one real (λ_1) and one complex conjugate pair (λ_2, λ_3) of eigenvalues. A vortex is inward ($\lambda_1<0$) or outward ($\lambda_1>0$) when axial components of trajectories move respectively toward or away from S. Also, it may be stable ($Re\{\lambda_2\}<0$), nilpotent ($Re\{\lambda_2\}=0$), or unstable ($Re\{\lambda_2\}>0$).

xx. When a vortex has $\lambda_1=0$ then it is called a center.

TABLE II
Behavior about S_{s2}

Parameter Variations → / ↓	$A>B$	$A=B$	$A<B$
$C>2(1+\sqrt{2})$	Unstable node	Unstable node	Unstable saddle
$0<C\leqslant 2(1+\sqrt{2})$	Outward unstable vortex	Unstable center	Inward unstable vortex
$C=0$	Outward nilpotent vortex	Nilpotent center	Inward nilpotent vortex

TABLE IIIA
Behavior about S_{s3}—case $B>1/8$

Parameter Variations → / ↓	$A>B$	$A=B$	$A<B$
$C\geqslant 0$	Inward stable[x] vortex	Stable center[x]	Outward stable vortex

TABLE IIIB
Behavior about S_{s3}—case $0\leqslant B\leqslant 1/8$

Parameter Variations → / ↓	$A>B$	$A=B$	$A<B$
$C>\left(\frac{1}{8B}-1\right)\sqrt{A/B}$	Inward stable[x] vortex	Stable center[x]	Outward stable vortex
$0\leqslant C\leqslant\left(\frac{1}{8B}-1\right)\sqrt{A/B}$	Stable node[x]	Stable node[x]	Stable saddle

x. Point has three-dimensional local stable manifold.

By inspecting the tables it is evident that the various stability conditions are determined by two parameters, C and B/A. This is convenient since it is possible to represent graphically Tables II and III as Figs 2 and 3. The first-order stability analysis about the three steady states is completed.

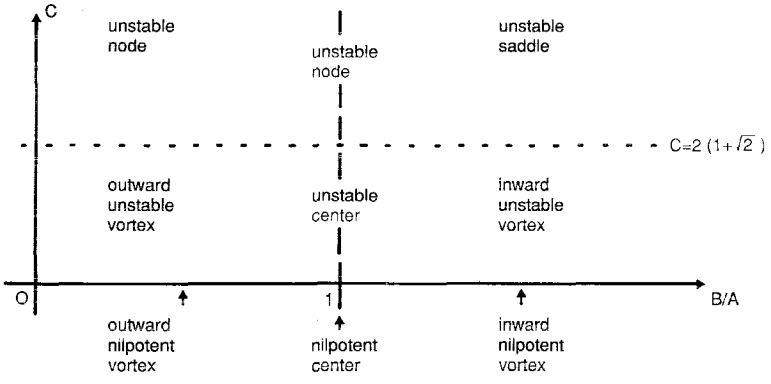

Figure 2. Behavior of S_{s2}, graphical presentation. (See Table II).

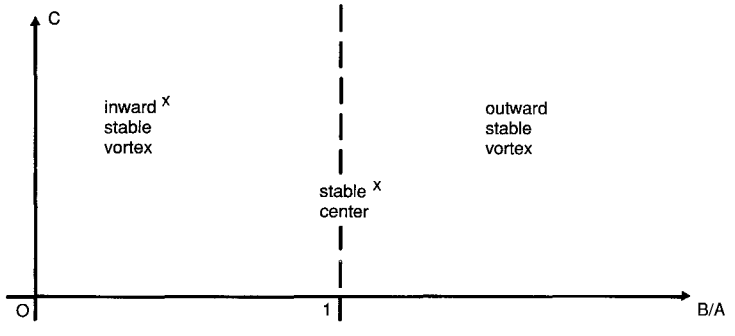

Figure 3a. Behavior of S_{s3}—case $B > 1/8$, graphical presentation. (See Table IIIa).

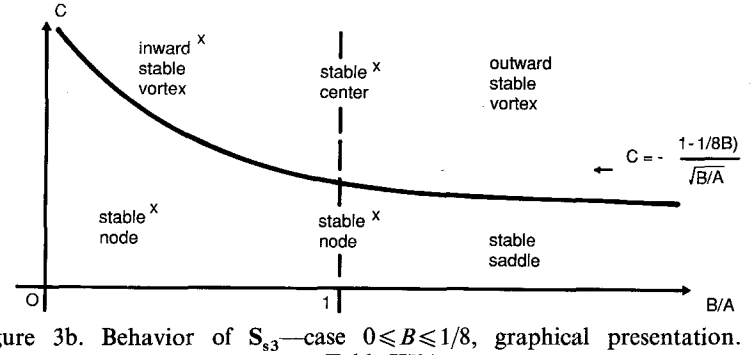

Figure 3b. Behavior of S_{s3}—case $0 \leqslant B \leqslant 1/8$, graphical presentation. (See Table IIIb).

Geometric properties. By examining (1) it is possible to deduce that Σ contains three two-dimensional subsystems, namely,

$$\dot{X}=X-XY+CX^2$$
$$\dot{Y}=-Y+XY \tag{5}$$

$$\dot{X}=X+CX^2-AZX^2$$
$$\dot{Z}=-BZ+AZX^2 \tag{6}$$

$$\dot{Y}=-Y$$
$$\dot{Z}=-BZ. \tag{7}$$

It is clear that the subsystems (5), (6) and (7), respectively are confined to $[X, Y]$, $[X, Z]$ and $[Y, Z]$ subspaces of $\mathbf{R}^3$. Thus, a solution of Σ initiated in any given subspace will remain confined to the same subspace. Also, observe that the three steady states are in these subspaces. See Fig. 1.

Now, let $\bar{\mathbf{P}}_u=\{[U]; U\geqslant 0 \text{ s.t. } U=X, Y, Z\}$ be the sets that define the positive intervals of X, Y and Z in $\mathbf{R}^3$. In addition, let $\bar{\mathbf{P}}_{xy}=\{[X, Y]; \text{s.t. } X, Y\geqslant 0\}$ be a set that defines the positive space of $[X, Y]$ in $\mathbf{R}^3$. Then by the positive open space of $[X, Y]$ in $\mathbf{R}^3$ we imply the set $\mathbf{P}_{xy}=\{\bar{\mathbf{P}}_{xy}-\bar{\mathbf{P}}_x\cup\bar{\mathbf{P}}_y\}$. Similarly, one can define $\mathbf{P}_{xz}$ and $\mathbf{P}_{yz}$. Furthermore, let $\bar{\mathbf{P}}^3=\{\mathbf{R}^3; \text{s.t. } X, Y, Z\geqslant 0\}$. Then the set $\mathbf{P}^3=\{\bar{\mathbf{P}}^3-\bar{\mathbf{P}}_{xy}\cup\bar{\mathbf{P}}_{xz}\cup\bar{\mathbf{P}}_{yz}\}$ defines the positive open space of $\mathbf{R}^3$ in which an important result exists.

Since Σ contains subsystems that are restricted to the two-dimensional subspaces $[X, Y]$, $[X, Z]$, and $[Y, Z]$, then any solution of (1) initiated in a given orthant of $\mathbf{R}^3$ will remain confined to the space of the same orthant. Thus, all solutions of Σ initiated in $\mathbf{P}^3$ will remain in $\mathbf{P}^3$ for all times. This fact is crucial when modeling chemical, biochemical, or ecological phenomena (Feinberg, 1980). The geometric property just analyzed will be referred to as the geometric separability of Σ.

To study the qualitative behavior of Σ in $\mathbf{P}^3$, one can investigate the stability properties of the three subsystems. The subsystem (5) is the Lotka–Volterra model and is confined to the $[X, Y]$ subspace of $\mathbf{R}^3$. The results of this system are well known and are reported in (Davis, 1962; Nicolis and Prigogine, 1977). The subsystem (7) represents a linear differential equation that is asymptotically stable in the $[Y, Z]$ subspace of $\mathbf{R}^3$. However, the subsystem (6) is nonlinear and is responsible for an interesting behavior of Σ. This system without the X term was studied by Tyson and Light (1973). By examining (6) it is concluded that in $\mathbf{P}_{xz}$ the system is always stable. This is observed while analyzing $\Gamma\{J(\mathbf{S}_{s3})\}$, $\mathbf{W}\{J(\mathbf{S}_{s3})\}$, Table III and Fig. 3. Note that the direction of instability for $\mathbf{S}_{s3}$ occurs through the first eigenvector in $\mathbf{W}\{J(\mathbf{S}_{s3})\}$, which punctures $\mathbf{P}^3$, and couples the effect to the Lotka–Volterra equation. See

Fig. 1. Furthermore, (6) contains the highest-order terms, which are of degree 3. This implies that for large values of $\|\mathbf{S}\|$, $\mathbf{S}\in\mathbf{P}^3$, the stability of Σ is dominated by the behavior of (6). To be more specific, in $\mathbf{P}^3$ the flow of (6) has the property to lift the unstable solutions of (5), and to either put them at rest in the steady state $\mathbf{S}_{s3}$, or to inject them via $\mathbf{S}_{s3}$ back to the Lotka–Volterra behavior. Therefore, whatever the local stabilities of steady states, Σ is always bounded in $\mathbf{P}^3$. Table IV summarizes above observations.

TABLE IV
Geometrically separable systems in Σ

Equations ↓	$\mathbf{P}_{xy}$	$\mathbf{P}_{xz}$	$\mathbf{P}_{yz}$	$\mathbf{P}^3$
Lotka–Volterra $\dot{X}=X-XY+CX^2$ $\dot{Y}=-Y+XY$	$C=0$, periodic $C>0$, unstable focus	no effect	no effect	1st and 2nd order effects
$\dot{X}=X+CX^2-AZX^2$ $\dot{Z}=-BZ+AZX^2$	no effect	stable	no effect	1st, 2nd and 3rd order effects
$\dot{Y}=-Y$ $\dot{Z}=-BZ$	no effect	no effect	asymptotic stability	1st order effect
Σ	$C=0$, periodic $C>0$, unstable focus	stable	asymptotic stability	bounded by 3rd order effects of equation (6)

We conclude this section by noting that the geometric separability of Σ implies that trajectories initiated in $\mathbf{P}^3$ always remain confined to it. If this were not so, the uniqueness of solutions of Σ would be violated, or the geometric separability would not hold.

Global Behavior of Σ *in* $\mathbf{P}^3$. The intrinsic growth and decay rate terms of Σ are $X+CX^2$, $-Y$ and $-BZ$. The remaining terms are feedback. $\dot{Y}$ and $\dot{Z}$ equations possess positive feedback terms XY and AZX^2, respectively, while the $\dot{X}$ equation has negative feedback terms $-XY$ and $-AZX^2$. Note that all feedback terms depend on X. Thus, X activates growth of Y and Z while Y and Z inhibit X. Moreover, the intrinsic growth and decay terms taken alone imply that X would experience unbounded growth while Y and Z would go to extinction. Y and Z cannot survive without preying on X while X cannot stay finite without limitation due to Y and Z. Hence, Σ is a two-predator and one-prey system where the predators Y, Z do not interact directly with one another but compete for prey X.

From these arguments it follows that the global behavior of Σ will depend on the behavior of $X(t)$ and feedback terms. For the large values of X, the $\dot{X}$ equation can be approximated by

$$\dot{X}=X^2(C-AZ) \tag{8}$$

since the lower order terms, attributed to the intrinsic growth rate and feedback, can be ignored. The solution of (8) is

$$X(t)=\frac{X_0}{1-X_0[C(t-t_0)-A\int_{t_0}^{t} Z(\tau)\,d\tau]} \tag{9}$$

where $X_0=X(t_0)$, and where $A\int Z(\tau)\,d\tau>0$ for all solutions in $\mathbf{P}^3$. The solution (9) offers two conditions:

$$\text{(i)}\quad C(t-t_0)>A\int_{t_0}^{t} Z(\tau)\,d\tau$$

$$\text{(ii)}\quad C(t-t_0)<A\int_{t_0}^{t} Z(\tau)\,d\tau.$$

Observe, the condition (i) implies that the solution of $X(t)$ may reach infinity in a finite time (Samardzija, 1983). However, this will never happen because of the following argument.

Suppose that we start Σ at a large value of X, and the condition (i) initially exists. Then $X(t)$ will increase rapidly, forcing the solutions $Y(t)$ and $Z(t)$ to do the same because of the positive feedback. This in turn will amplify the negative feedback on the species X and will force the condition (ii) to occur, and thus prevent $X(t)$ from escaping in a finite time (Samardzija, 1983). The negative feedback will start decreasing $X(t)$, and this will reduce the amount of the positive feedback in Σ. The latter will force $Y(t)$ and $Z(t)$ to decrease also. If now $Z(t)$ decreases to the point that the condition (i) is reached again, the solutions will start growing until the condition (ii) occurs. Thus, a trajectory can repeatedly go through the conditions (i) and (ii), which will force Σ to oscillate in $\mathbf{P}^3$. However, if solutions reach the condition (ii) that remains satisfied for all times, then trajectories will end in steady state. In any event Σ will be bounded.

2. Bifurcation and Stability Properties.

Stability diagrams. Since the behavior of Σ is bounded in $\mathbf{P}^3$ then the solutions of (1) cannot reach infinity in any finite or infinite time. Therefore, the behavior of Σ in $\mathbf{P}^3$ is determined by the behavior of three steady state solutions. $\mathbf{S}_{s1}$ is always a saddle point, implying that the trajectories will repel

from it for all values of A, B and C. However, $\mathbf{S}_{s2}$ and $\mathbf{S}_{s3}$ have different behavior as parameters are varied and, therefore, will influence trajectories in different ways. By superimposing Figs 2 and 3a and Figs 2 and 3b, stability diagrams are obtained as illustrated in Figs 4, 5 and 6. These diagrams describe the effects of $\mathbf{S}_{s2}$, $\mathbf{S}_{s3}$, and boundedness of $\boldsymbol{\Sigma}$ on trajectories in $\mathbf{P}^3$. The various stability regions are indicated in the diagrams. Before we continue with investigation of these regions, the bifurcation mechanism that is responsible for stability changes in $\boldsymbol{\Sigma}$ will be addressed.

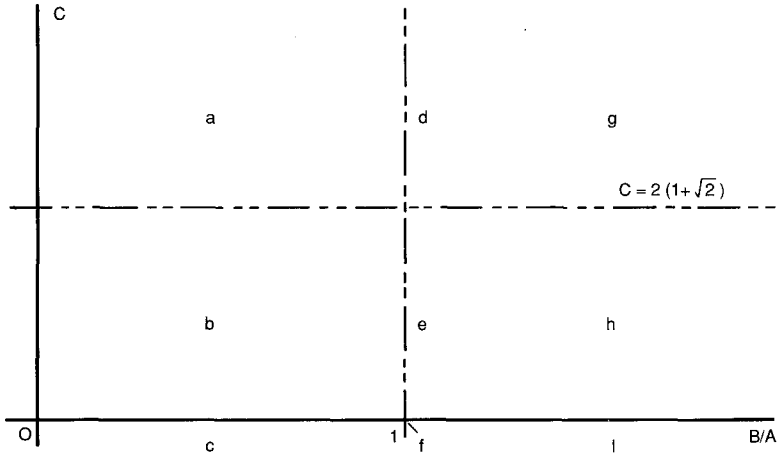

Figure 4. Superposition of Figs 2 and 3a, case $1/8 < B$—stability diagram.

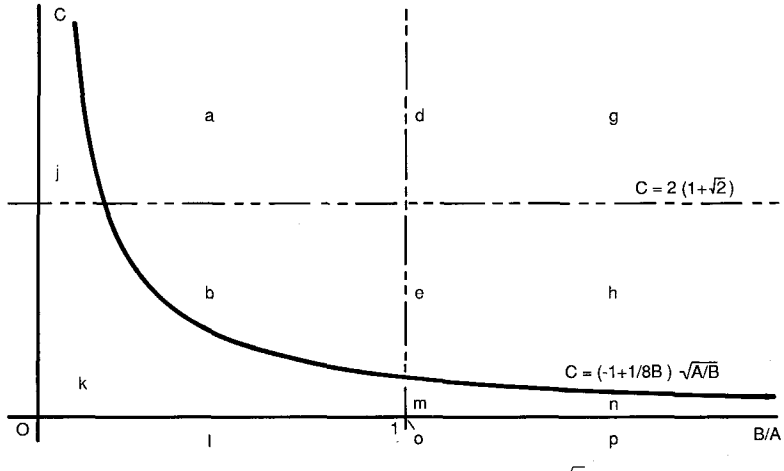

Figure 5. Superposition of Figs 2 and 3b, case $1/(8(3+\sqrt{2})) \leqslant B \leqslant 1/8$—stability diagram.

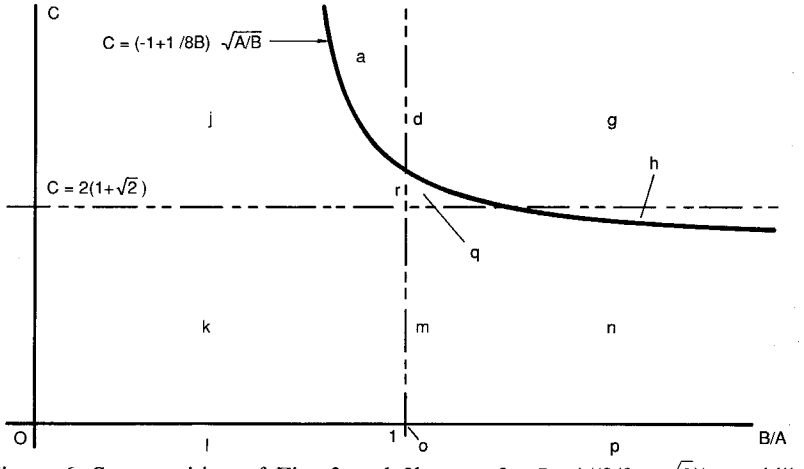

Figure 6. Superposition of Figs 2 and 3b, case $0 \leqslant B \leqslant 1/(8(3+\sqrt{2}))$—stability diagram.

Bifurcation mechanisms in Σ. It is important to note that the steady state S_{s1} does not play any role in the bifurcation scheme of Σ. S_{s1} is always a saddle of index 1 and can be viewed as an artifact of the geometric separability. Thus, bifurcation must be associated with the behavior of two other steady states.

By examining S_{s2} and S_{s3} one can see that the eigenvalue real parts of the vortices never change signs as B/A is varied. For example, in Fig. 3a $Re\{\lambda\}$ of S_{s3} is always negative implying a stable vortex. Thus, the bifurcation mechanism must be activated by the pure real eigenvalues that correspond to the first elements in $\Gamma\{J(S_{si})\}$ $i=2, 3$. These eigenvalues determine insets and outsets of the two vortices. This eliminates a possibility for the Hopf-type bifurcation when just B/A is varied. For the reasons which will be apparent later, the bifurcation which occurs at $B/A=1$ will be referred to as the non-transversal saddle connection type.

If C is allowed to be negative as well as positive then a supercritical Hopf-type bifurcation at S_{s2} occurs across the line $C=0$ and for $B/A>1$. This is easily observed by inspecting $\Gamma\{J(S_{s2})\}$. In fact, the line $C=0$ represents the critical Hopf region. But, this analysis is outside the scope of this paper since it is assumed that $C \geqslant 0$.

There is one more important property of vortex type complexes in Σ. By examining the sets $\Gamma\{J(S_{si})\}$, $i=2, 3$ the following conclusions can be reached. The complex eigenvalues are always associated with eigenvectors that define the rotation in P_{xy} or P_{xz}, while the pure real eigenvalues are associated with eigenvectors transverse to P_{xy} and P_{xz}. This implies that the purely real eigenvalues, hence vortex axial motions, are created through the interactions of all species in Σ, while the rotational aspects of the vortices are generated by interactions of X, Y or X, Z species.

Stability regions. Let us now look at some of the stability regions in Figs 4, 5, 6. For example, in the region **a**, $\mathbf{S}_{s2}$ is an unstable node and $\mathbf{S}_{s3}$ is an inward stable vortex. Thus, $\mathbf{S}_{s2}$ is the repellor or source, while $\mathbf{S}_{s3}$ is the attractor or sink. This implies that all trajectories in $\mathbf{P}^3$ will be attracted to rest at $\mathbf{S}_{s3}$. Hence, $\boldsymbol{\Sigma}$ is stable in $\mathbf{P}^3$. On the other hand, in the region **p** which is defined for $B/A>1$ and along the line $C=0$, $\mathbf{S}_{s2}$ is an inward nilpotent vortex and $\mathbf{S}_{s3}$ a stable saddle (source), i.e. a saddle of index 1. Here, $\mathbf{S}_{s2}$ attracts all solutions in $\mathbf{P}^3$ toward the $[XY]$-plane that supports periodic orbits. Thus, a trajectory in $\mathbf{P}^3$ either approaches a periodic orbit in the $[XY]$-plane, or $\mathbf{S}_{s2}$ itself. Consequently, in the region **p** one has periodic or steady state solutions. The outcome depends on the parameter B/A and the initial conditions selected. In these examples we note that once the condition (ii) takes over the global behavior, then it remains in force until the system is at rest, or until the system converges to the conservative Lotka–Volterra solutions.

An interesting behavior arises in the region **h**. Here $\mathbf{S}_{s3}$ and $\mathbf{S}_{s2}$ are respectively outward stable (index 1 saddle focus) and inward unstable (index 2 saddle focus) vortices. This implies now that all the steady state points are repellors. Thus, since there are no sinks in $\mathbf{P}^3$ and yet $\boldsymbol{\Sigma}$ is bounded, the formation of periodic or chaotic type trajectories is expected. We shall elaborate more on this in the next section.

By proceeding with analysis of each region in the fashion outlined above, one can reach the following conclusions:

Stable steady state regions are **a**, **b**, **c**, **d**, **e**, **f**, **j**, **k**, **l**, **m**, **o** and **r**.

Periodic/stable steady state regions are **i** and **p**.

Chaotic/periodic regions are **g**, **h**, **n** and **q**.

Therefore, stable solutions are generated left of and including the line $B/A=1$ while the chaotic or periodic solutions exist to the right of the line $B/A=1$. An exception is the region $B/A>1$ along the line $C=0$ where the periodic or attracting steady state solutions may exist, and this region is associated with the supercritical Hopf bifurcation.

Non-transversal saddle connection bifurcation, fractal torus and explosive route to chaos. Since we have determined the behavior to the left and right of the line $B/A=1$, the question is now what conditions exist at the line itself. By setting $B/A=1$ and equating the right side of $\boldsymbol{\Sigma}$ to zero, the singular points are determined. One of the solutions is $L=\{(X, Y, Z);\ \text{s.t.}\ X=1 \text{ and } Y+AZ=1+C\}$. This solution is a one-dimensional invariant manifold parallel to the $[YZ]$-plane at $X=1$ and passing through $\mathbf{S}_{s2}$ and $\mathbf{S}_{s3}$. All points along L are singular. Hence, no motion exists along it.

If now one moves in parameter space to the left of $B/A=1$, the manifold L exerts flow toward the inward stable vortex or stable node defined by $\mathbf{S}_{s3}$. However, if we move to the right of $B/A=1$, the manifold L exerts the motion

toward the inward unstable vortex or index 2 saddle defined by $\mathbf{S}_{s2}$. Consequently, the line $B/A=1$ in parameter space is critical since by passing through it the system changes behavior. From now on, only the behavior to the right of $B/A=1$ will be considered.

As mentioned earlier, the region **h** near $B/A=1$ contains the inward unstable ($\mathbf{S}_{s2}$) and outward stable ($\mathbf{S}_{s3}$) vortices. Hence, the situation is very similar to a non-transversal saddle connection between two saddles with indices 2 and 1 (Abraham and Shaw, 1985). Now, because the solutions cannot be stabilized at $\mathbf{S}_{s2}$, they are by the vortex action injected back into $\mathbf{P}^3$ (rebirth of Z). But, the boundedness of Σ will confine their motion and condition (ii) will force the flow toward $\mathbf{S}_{s3}$ (near extinction of Y). Near $\mathbf{S}_{s3}$, the outset (rebirth of Y) will re-direct the flow toward $\mathbf{S}_{s2}$ (near extinction of Z). The process repeats itself. One can easily conclude that this behavior results in oscillations. It is worth noting that the one-dimensional outset of $\mathbf{S}_{s3}$ and the one-dimensional inset of $\mathbf{S}_{s2}$ can be viewed as the coupling and mixing mechanism of two frequencies characterizing vortices at $\mathbf{S}_{s3}$ and $\mathbf{S}_{s2}$.

Similar dynamics occurs in the regions **g** and **n**. The only difference is that one of the steady solutions looses complex eigenvalues. In the region **q**, however, all steady state solutions have pure real eigenvalues, and yet oscillatory behavior exists. It is as if rotational flow information is lost before the flow reaches the neighborhood of steady state points. In any event, the non-transversal arrangements of insets and outsets at $\mathbf{S}_{s2}$ and $\mathbf{S}_{s3}$ and boundedness of Σ are responsible for oscillatory behavior in all four regions. Observe the different non-transversal arrangements of insets and outsets at the right and left of $B/A=1$.

In order to visualize the oscillatory behavior in the regions considered, Σ was numerically integrated on a CRAY-1A machine running CRAY FORTRAN version 1.14. Integration of the differential equations employed the Gear method (1971) for stiff ordinary differential equations as implemented in the IMSL subroutine DGEAR with 10^{-8} relative error tolerance. CRAY FORTRAN provides approximately 14 decimal digits of precision in the range $10^{\pm 2466}$. The results for the four regions were computed and are illustrated in Figs 7, 8, 9 and 10. Figure 11 illustrates an analog simulation which supports digital results. With exception of Fig. 11, all other figures exhibit only a few cycles around the attractor. This was done so that a visualization of attracting sets is more clear. If a large number of cycles are plotted, the attractors would be filled as seen in Fig. 11 and one would not see the behavior. The solutions presented are chaotic and no periodic or quasiperiodic solutions were detected close to the line $B/A=1$. All attractors expose the connecting straight "line" L, which is organized by the non-transversal arrangement of outset and inset manifolds. This "line" does not represent a unique trajectory, however. Instead, it can be viewed as the manifold in which the phase space around vortices

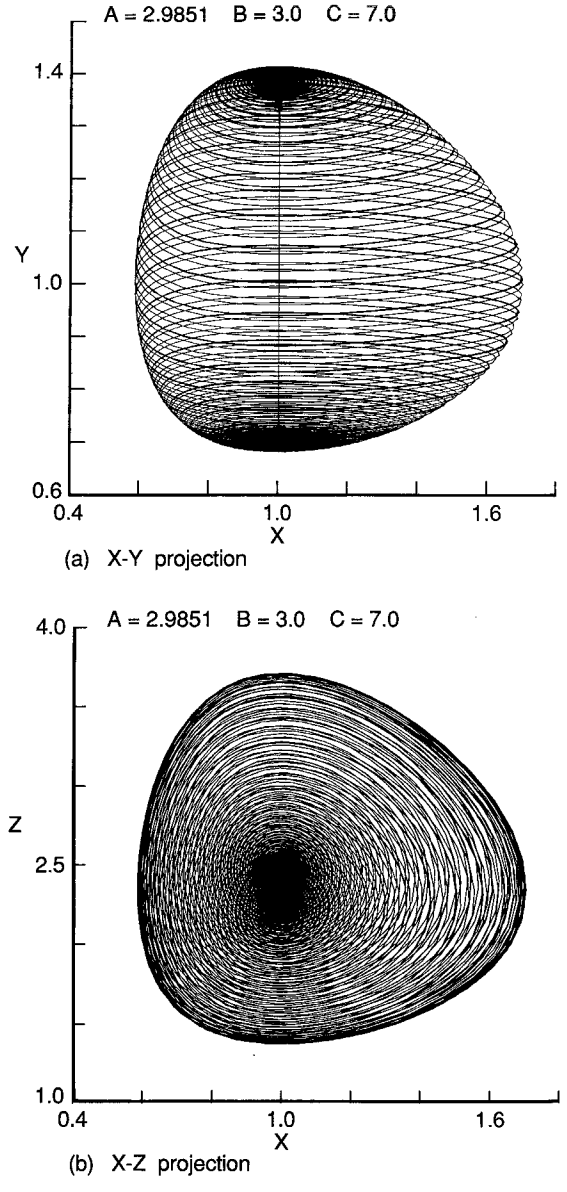

Figure 7. Chaotic attractor in region **g**. X–Y projection and X–Z projection.

collapses into a dense bundle of trajectories. This "line" exhibits the slowest dynamics on the attractor and is referred to as the slow manifold. In fact, the motion along this manifold is quite similar to Shaw's dripping faucet dynamics (Gleick, 1987). The fast manifold is the outer shell of the attractor. Observe, the slow and fast manifolds result from heteroclinic tangles induced by stable and unstable manifolds characterizing singular points $\mathbf{S}_{s2}$ and $\mathbf{S}_{s3}$.

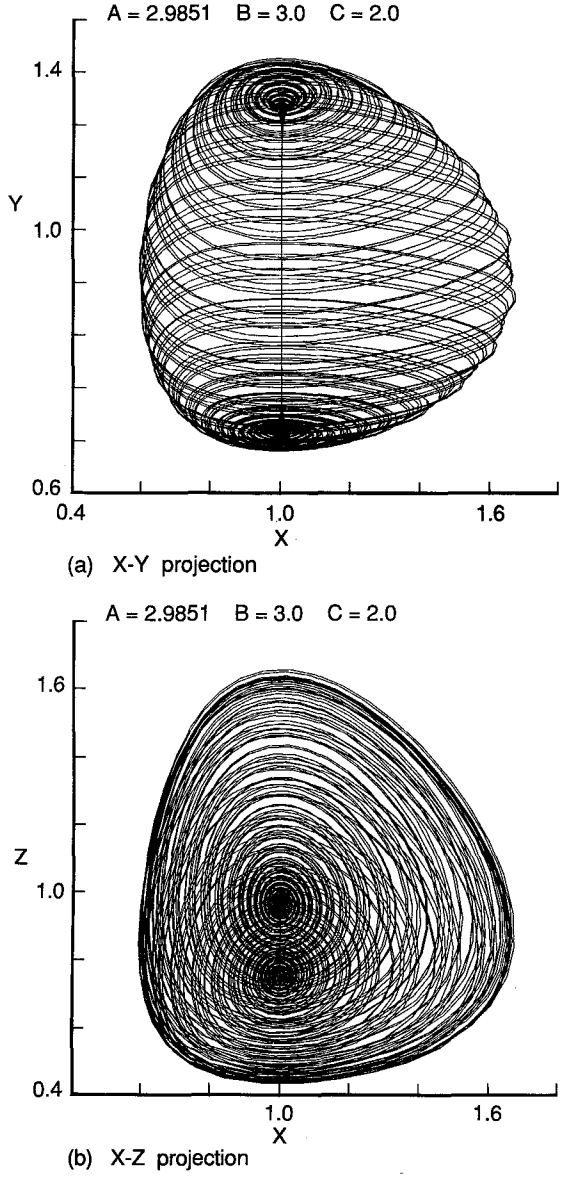

Figure 8. Chaotic attractor in region **h**. X–Y projection and X–Z projection.

But this is precisely the Birkhoff–Smale criteria for existence of turbulence (Hale; Smale, 1966). Note, as B/A is increased the slow manifold opens into a hole, and chaotic attractors evolve into a conventional toroidal shape.

In order to verify the chaotic nature of solutions, one can take advantage of the slow manifold in the following way. Suppose one cuts transversely the manifold with a Poincaré plane and records interarrival times of trajectories

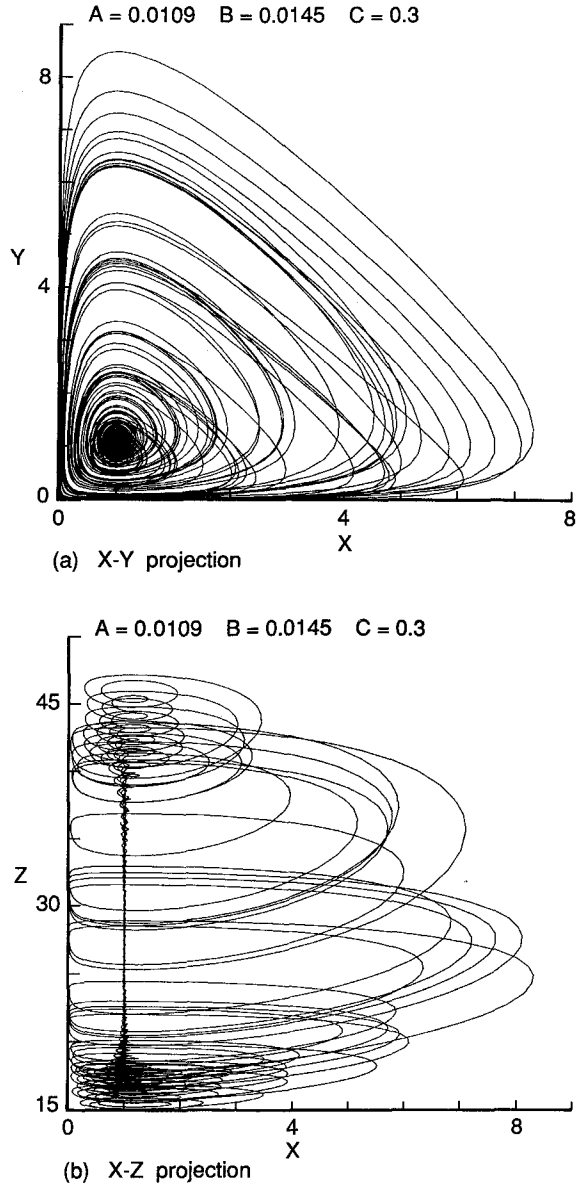

Figure 9. Chaotic attractor in region **n**. X–Y projection and X–Z projection.

piercing the plane. This is analogous to measuring with laser light droplet interval times of water from a dripping faucet (Shaw). Then, if interarrival times are plotted against the intersection number, the interarrival time diagram is obtained. The interarrival time return map (Δt_{n+1} vs Δt_n) can be constructed from the same data (Shaw).

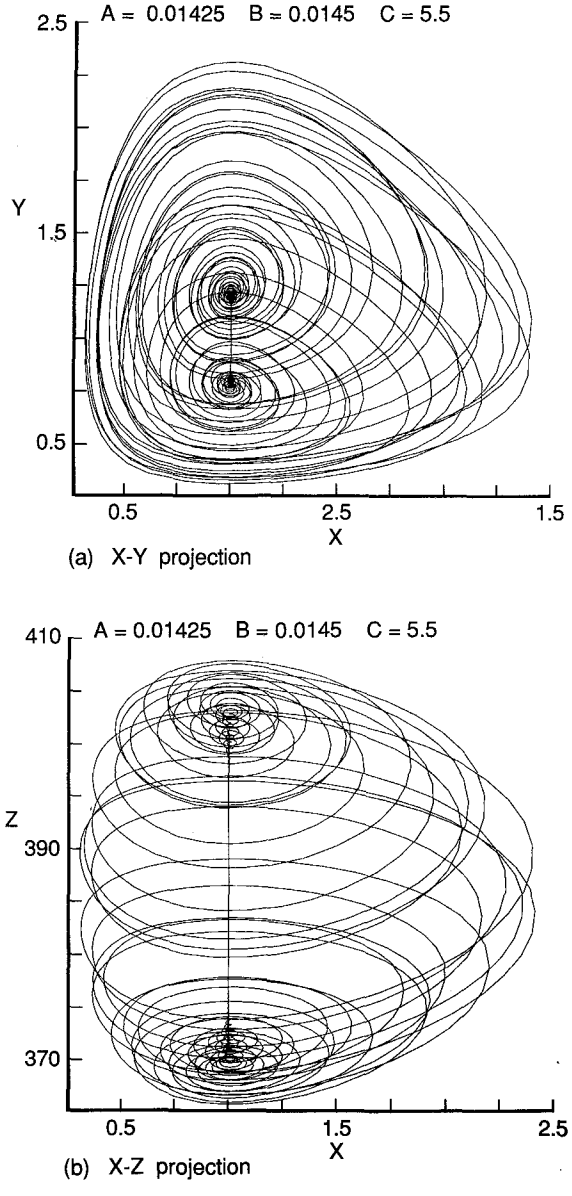

Figure 10. Chaotic attractor in region **q**. X–Y projection and X–Z projection.

For this test we selected the attractor of Fig. 7 which may appear to support quasiperiodic solutions. The results are presented in Figs 12a and 12b. These figures are constructed from a large number of cycles and indicate the stochastic behavior analogous to Shaw's dripping faucet experiments. Hence, the attractor of Fig. 7 is a chaotic attractor. In fact, all attractors illustrated are

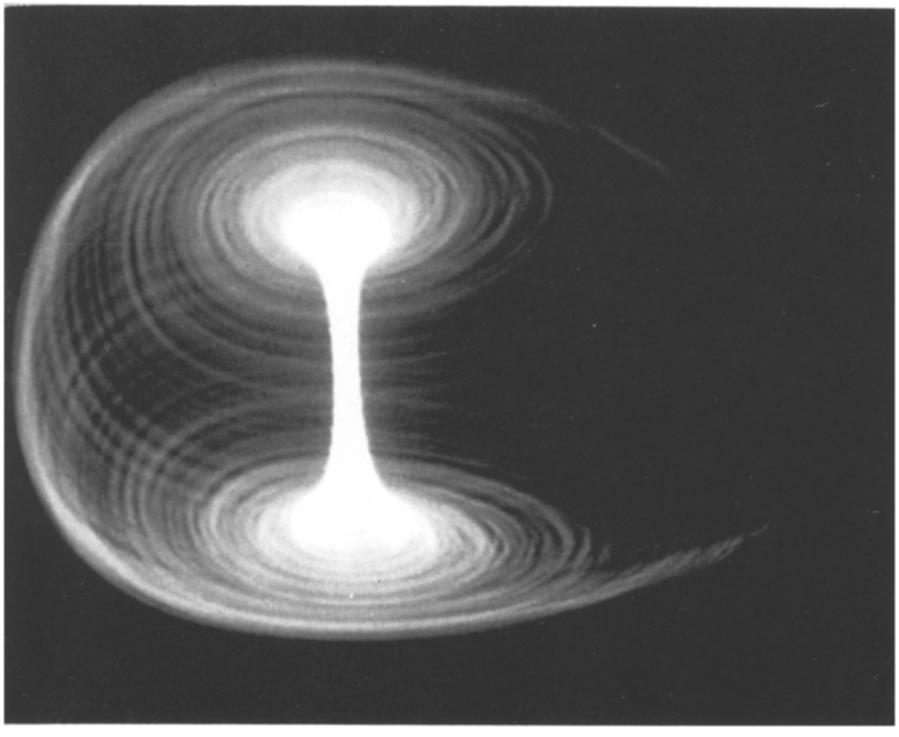

Figure 11. Analog similation of chaotic attractor in the region **h**.

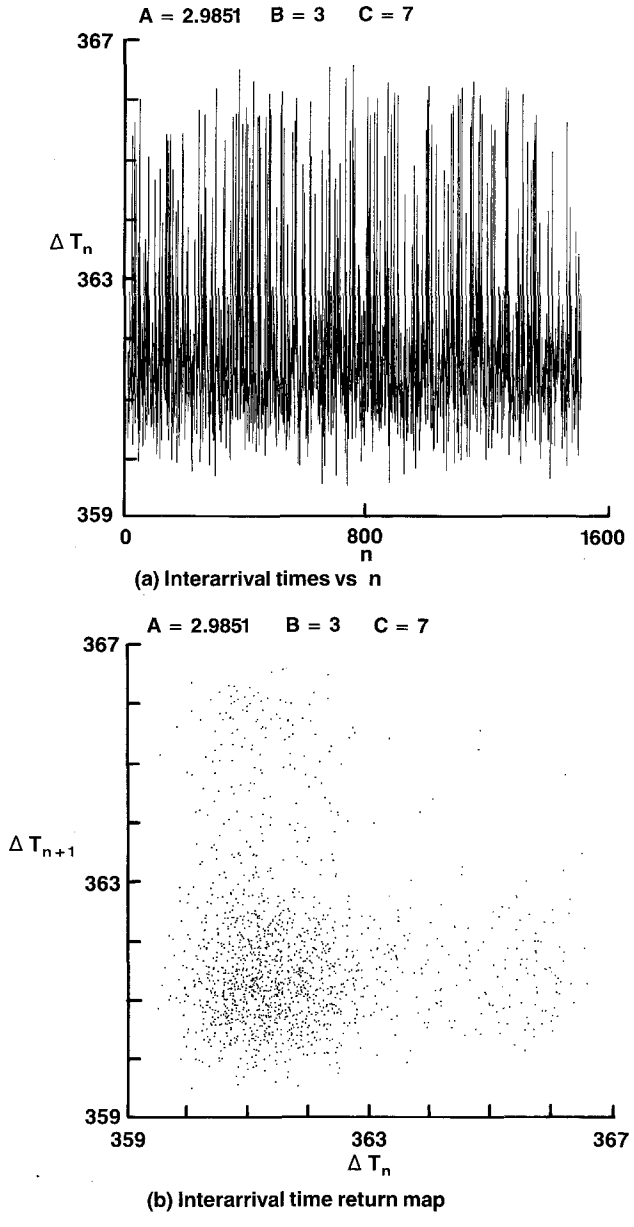

Figure 12. (a) Interarrival time diagram for the attractor in Fig. 7. (b) Interarrival time return map obtained from data in Fig. 12a.

chaotic. This also can be verified by computing the Poincaré section. For example, in Fig. 13 the Poincaré section for the attractor indicated is shown. This section is constructed in the usual manner by plotting Z intersection vs X intersection of a trajectory piercing a Poincaré surface. The Poincaré surface selected is a two-dimensional manifold in $\mathbf{R}^3$ with normal along the Y-axis and

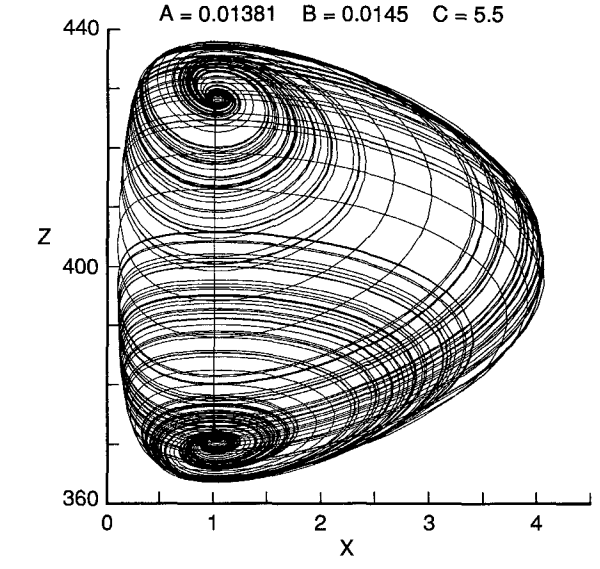

(a) X-Z projection of attractor

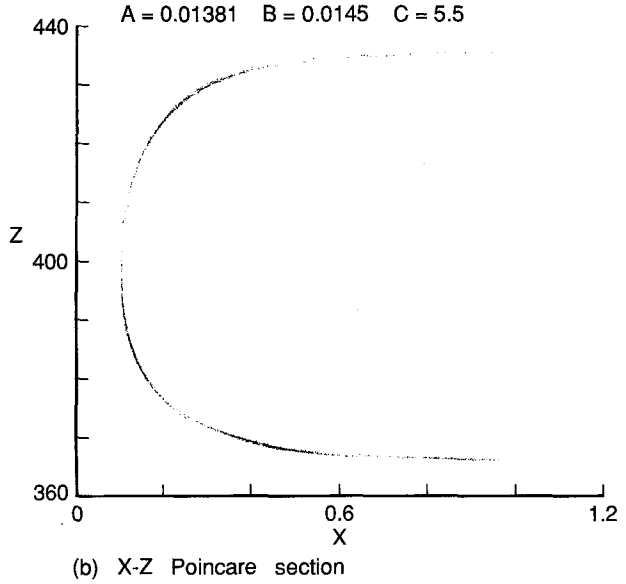

(b) X-Z Poincare section

Figure 13. Poincaré section. X–Z projection of attractor and X–Z section.

originating at $Y=1$. Only intersections for which trajectories cross in the decreasing-Y direction are recorded. Observe the thickening of the horseshoe shape that arises due to a fractal nature of the attractor.

The chaotic attractor discussed is known as the fractal torus (Richetti *et al.*, 1987). The fractal torus due to these authors' results from the supercritical

Hopf-hysteresis type bifurcation; see also Guckenheimer and Holmes (1983), p. 396. Hence, its birth differs from the scheme described for Σ. However, if C is allowed to be negative and positive then the bifurcation scheme similar to that of the Bordeaux group exists across the line $C=0$ and for $B/A>1$. We also observe that their fractal torus is not confined to $\mathbf{P}^3$, thus it cannot represent directly real biological or chemical dynamics.

Finally, by consolidating the analysis of behavior about $B/A=1$, one concludes that Σ *jumps out of the steady state solution directly into the chaos through the birth of a fractal torus!* This type of scenario is referred to as the *explosive route to chaos*. In this scenario there are *no periodic or quasiperiodic transitions between the steady state and chaotic regions.*

3. Kinetics and Generalization.

A kinetic scheme for Σ. One possible kinetic scheme for Σ can be written as:

$$\begin{aligned} &[D]+X\rightarrow 2X \quad (R1)\\ &X+Y\rightarrow 2Y \quad (R2)\\ &Y\rightarrow P1 \quad (R3) \end{aligned} \tag{8a}$$

$$\begin{aligned} \Delta:\ &[c]+2X\rightarrow 3X \quad (R4)\\ &2X+Z\rightarrow 3Z \quad (R5)\\ &Z\rightarrow P2 \quad (R6). \end{aligned} \tag{8b}$$

[ ] means concentrations are supplied in significant excess; hence, these quantities are constant. All rate constants are unity except for reactions $R1$, $R5$ and $R6$ where $k1=1/[D]$, $k5=A/2$ and $k6=B$. X, Y and Z are reacting intermediates. $P1$ and $P2$ are nonreacting products.

Reactions $R1$–$R3$ are the classic 1920 Lotka (1920) mechanism. It is well known that this mechanism is a conservative oscillatory dynamical system. Reactions $R4$–$R6$ constitute the Tyson and Light (1973) trimolecular Lotka–Volterra oscillator, hereafter referred to as TLLV. Scheme Δ can represent kinetics phenomenologically if desired so that the trimolecular step $R5$ can represent any sequence of elementary steps where the net rate of production of Z and consumption of X is proportional to ZX^2.

Consulting Table V, it is clear that one interpretation for Σ is a TLLV mechanism in (X, Z) coupled through X to a classic Lotka mechanism in (X, Y). Though kinetic scheme Δ can be partitioned formally into these two kinetic scheme subsystems, the geometric separability of Σ into subsystems (5), (6) and (7) involves mixtures of terms from *both* kinetic scheme subsystems. Thus, the behavior that emerges from Σ is *not* a simple combination of the behaviors from Lotka and TLLV schemes considered separately. Much richer behavior emerges from Σ.

TABLE V

Reaction ↓		Rate constant	Terms contributed to ... $\dot{X}$	$\dot{Y}$	$\dot{Z}$
$[D]+X\rightarrow 2X$		$1/[D]$	X	—	—
$X+Y\rightarrow 2Y\Rightarrow$	Lotka (1920)	1	$-XY$	XY	—
$Y\rightarrow P1$		1	—	$-Y$	—
$[C]+2X\rightarrow 3X$	Tyson and	1	CX^2	—	—
$2X+Z\rightarrow 3Z\Rightarrow$	Light (1973)	$A/2$	$-AZX^2$	—	AZX^2
$Z\rightarrow P2$	(*TLLV*)	B	—	—	$-BZ$

C, D in excess.

For example, even the local behavior about a steady state of the TLLV can be altered by being embedded in Σ. Tyson and Light (1973) show that TLLV with $A=B=1$ has a positive $[X, Z]$ steady state $[X_0, Z_0]^T=[1, C]^T$. It is a center, i.e. the two eigenvalues of $[X_0, Z_0]^T$ are complex conjugate with zero real parts. In Σ, however, because of the coupling of the Lotka and TLLV mechanisms, this steady state is $\mathbf{S}_{s3}=[X_0, T_0, Z_0]^T=[1, 0, 1+C]^T$ when $A=B=1$. More importantly, this steady state in Σ is *attracting* in the $[X, Z]$-plane. The complex conjugate eigenvalues corresponding to the $[X, Z]$-plane eigenvectors have negative, not zero, real parts (equation (4) and Table IIIa).

Higher order generalization of Σ. Σ, as well as the results obtained, can be generalized by introducing higher orders of biological interactions. The generalized system is of the form:

$$\dot{X}=X\prod_{i=1}^{n}(p_i-Y)+CX^j-AZX^{n+1},\quad 2\leqslant j\leqslant n+1$$

$$\mathbf{G\Sigma}:\quad \dot{Y}=-Y\prod_{i=1}^{n}(r_i-X)$$

$$\dot{Z}=-BZ+AZX^{n+1}$$

where n is odd, and $p_i, r_i>0$ for all i. $\mathbf{G\Sigma}$ has one steady state solution in the $[XZ]$-plane, and n^2 steady state solutions in the $[XY]$-plane. Now, let SP and VS define the number of saddle points and vortex type singularities that $\mathbf{G\Sigma}$ supports in the $[XY]$-plane. Then in the $[XY]$-plane one has $0\leqslant SP\leqslant(n^2-1)/2$ and $1\leqslant VS\leqslant(n^2+1)/2$, where the inequality signs take into account possible multiplicities of the factors associated with polynomials in the $\dot{X}$ and $\dot{Y}$ equations. For some of the possible topological configurations among the singular points in the $[XY]$-plane, see Arnold (1984, Figure 25). One should keep in mind that there is always a saddle point at the origin, but that one is not accounted for in SP.

It can also be shown that the system has up to n (depending on multiplicities) critical bifurcation points. This is accomplished by evaluating the Jacobian at the steady state point in the $[XZ]$-plane. The Jacobian is then examined for its singular solutions. The first point occurs at $(B/A)^{1/(n+1)} = r_{\min}$, where $r_{\min}$ is the smallest root of the polynomial in the $\dot{Y}$ equation, and other points follow in an ascending order of roots. $\mathbf{G\Sigma}$ also produces the explosive route to chaos. However, the shape of fractal tori is in general more complex than in the case of $\mathbf{\Sigma}$.

4. Observations and Conclusions. In order to get a more complete picture of $\mathbf{\Sigma}$'s behavior we used digital integration to compute bifurcation diagrams illustrated in Fig. 14. These diagrams are created by setting $C=5.5$ and $B=0.0145$ while varying the parameter A. This represents a slice through the regions **q** and **g** in Fig. 6. The diagrams display for a fixed values of B/A, $\log_{10} X$ or $\log_{10} Z$ from 100 intersections of a trajectory with a Poincaré surface transverse to the Y axis. The first 20 intersections are discarded before recording the next 100 intersections to allow short-term transients to die out. The Poincaré surface is a two-dimensional manifold in $\log_{10}(X, Y, Z)$-space with normal along the Y-axis and originating at $Y=1$. Intersections are noted only when a trajectory crosses the Poincaré surface in the decreasing-Y direction. After 100 intersections are recorded beyond the first 20 for a particular B/A-value, B/A is incremented by 0.005 where $B/A \in [1.005, 2.5]$. B is fixed and A is changing. As can be seen from Fig. 14, chaotic type solutions exist in the immediate right neighborhood of the line $B/A=1$, indicating the explosive nature of the scenario. However, the chaotic–periodic sequences do develop for $B/A > 1.45$. That is, in order to cross from the region of stable solutions into the region of chaotic–periodic sequences one has to go through a fractal torus. A similar qualitative behavior has been observed in data collected during the Belousov–Zhabotinskii chemical reaction experiments (Turner *et al.*, 1981; Argoul *et al.*, 1987). In fact, the Bordeaux group uses the fractal torus theory to explain this chemical reaction (Richetti *et al.*, 1987).

The system described in this paper suggests that it is a reasonable biological or chemical model. For example, Schaffer (1985) studies non-periodic fluctuations in the density of Canadian lynx. The results he presents do not appear to have a fractal torus structure. This may be because his model describes a one-predator/two-prey scheme. The $\mathbf{\Sigma}$ model also offers a generalization that allows higher-order biological or chemical terms. This may be of interest for cases where biological systems experience cataclysmic changes.

The authors wish to thank E. Wasserman for his encouragement, support and comments on this manuscript. We also wish to recognize suggestions from the referees of this work.

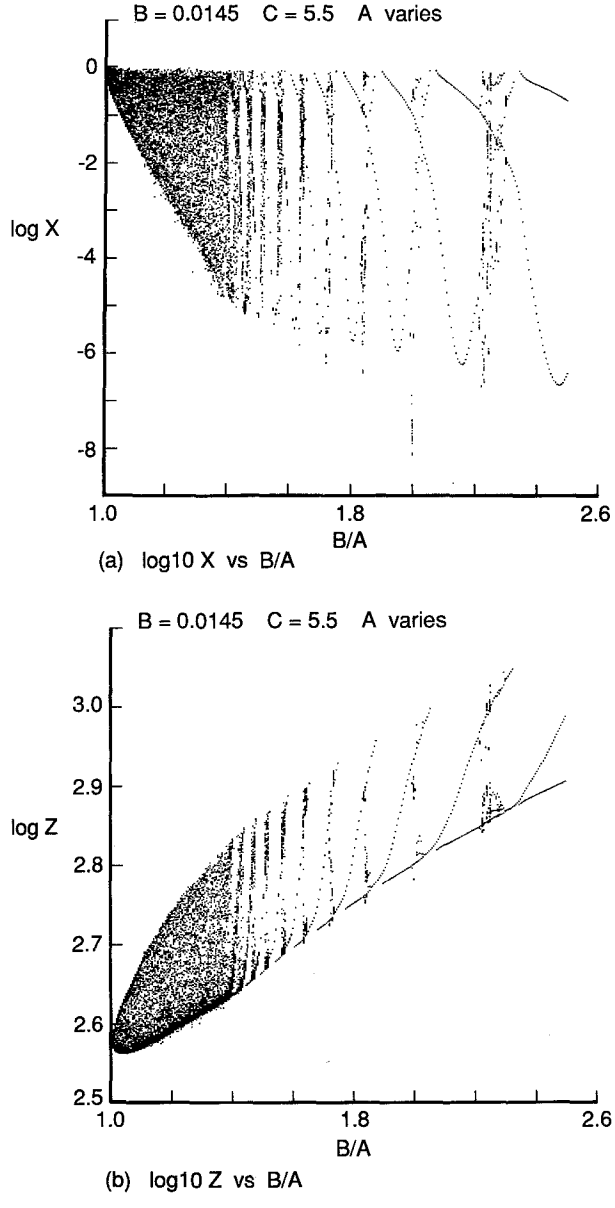

Figure 14. Bifurcation diagrams for the case $C=5.5$, $B=0.0145$ and A varies. (a) $\log_{10}(X)$ vs B/A. (b) $\log_{10}(Z)$ vs B/A.

LITERATURE

Abraham, R. H. and C. D. Shaw. 1985. *Dynamics—The Geometry of Behavior, Part 3*. Aerial Press, Inc., P.O. Box 1360, Sanata Cruz, California 95061.

Argoul, F., A. Arnéodo, P. Richetti and J. C. Roux. 1987. "From Quasiperiodicity to Chaos in the Belousov–Zhabotinskii Reaction I. Experiment." *J. chem. Phys.* **86** (6), 3325.

Arnéodo, A., P. Coullet and C. Tresser. 1980. "Occurrence of Strange Attractors in Three-dimensional Volterra Equation." *Phys. Lett.* **79A**, 259–263.
Arnéodo, A., P. Coullet, J. Peyraud and C. Tresser. 1982. "Strange Attractors in Volterra Equations for Species in Competition." *J. math. Biol.* **14**, 153–157.
Arnold, V. I. 1984. *Catastrophe Theory*. Springer-Verlag.
Davis, H. T. 1962. *Introduction to Nonlinear Differential and Integral Equations*. Dover.
Devaney, R. L. 1987. "Chaotic Bursts in Nonlinear Dynamical Systems." *Science* **235**, 342.
Feinberg, M. 1980. "Chemical Oscillations, Multiple Equilibria, and Reaction Networks." In *Dynamics and Modeling of Reactive Systems*. Ray, Stewart and Conley (Eds), Academic Press.
Gardini, L., C. Mammana and M. G. Messia. 1986. "Bifurcations in Three-Dimensional Lotka–Volterra Competitive Models." *Adv. Modelling and Simulation* **5** (3), 7–14.
Gear, C. W. 1971. *Numerical Initial Value Problems in Ordinary Differential Equations*. Englewood Cliffs, NJ.
Gilpin, M. E. 1979. "Spiral Chaos in a Predator–Prey Model." *Amer. Naturalist* **113**, 301–306.
Gleick, J. 1987. *CHAOS—Making a New Science*. Viking Penguin, Inc.
Guckenheimer, J. and P. Holmes. 1983. *Nonlinear Oscillations, Dynamical Systems and Bifurcations of Vector Fields*. Springer-Verlag.
Hale, J. K. *Topics in Dynamic Bifurcation Theory*. American Math. Soc., Providence, Rhode Island, No. 47.
IMSL Library Fortran Subroutines, IMSL Inc., Houston, Texas.
Lorenz, E. N. 1963. "Deterministic Non-Periodic Flows." *J. atmos. Sci.* **20**, 130–141.
Lotka, A. J. 1920. "Undamped Oscillations Derived from the Law of Mass Action." *J. Am. Chem. Soc.* **42**, 1595.
May, R. W. and W. J. Leonard. 1975. "Nonlinear Aspects of Competition between Three Species." *SIAM J. Appl. Math.* **29** (2), 243–253.
Nicolis, G. and I. Prigogine. 1977. *Self-Organization in Nonequilibrium Systems—From Dissipative Structures to Order through Fluctuations*. John Wiley.
Richetti, P., J. C. Roux, F. Argoul and A. Arnéodo. 1987. "From Quasiperiodicity to Chaos in the Belousov–Zhabotinskii Reaction II—Modeling and Theory." *J. chem. Phys.* **86** (6), 3339.
Rössler, O. E. 1976. "Chaotic Behavior in Simple Reaction System." *Z Naturforschung* **31a**, 259–264.
Samardzija, N. 1983. "Stability Properties of Autonomous Homogeneous Polynomial Differential Systems." *J. Diff. Equations* **48** (1), 60–70.
Schaffer, W. M. 1985. "Order and Chaos in Ecological Systems." *Ecology* **66** (1), 93–106.
Shaw, C. D. *The Dripping Faucet as a Model Chaotic System*. Aerial Press, Inc., P.O. Box 1360, Santa Cruz, California 95061.
Smale, S. 1966. "Structurally Stable Systems are not Dense." *Amer. J. Math.* **88**, 491–496.
Smale, S. 1976. "On the Differential Equations of Species in Competition." *J. math. Biol.* **3**, 5–7.
Sparrow, C. 1982. *The Lorenz Equations: Bifurcations, Chaos, and Strange Attractors*. Springer-Verlag.
Turner, J. S., J. C. Roux, W. D. McCormick and H. L. Swinney. 1981. "Alternating Periodic and Chaotic Regimes in a Chemical Reaction—Experiment and Theory." *Phys. Lett.* **85A**, 9–12.
Tyson, J. J. and J. C. Light. 1973. "Properties of Two-component Bimolecular and Trimolecular Chemical Reaction System. *J. chem. Phys.* **59** (8), 4164.
Volterra, V. 1931. "Leçons sur la Théorie Mathématiques de la Lutte pour la Vie." Paris.

Received 24 August 1987
Revised 20 January 1988